


Mimicking tetravalent dopant behavior using paired charge compensating dopants to improve the redox performance of ceria for thermochemically splitting H₂O and CO₂

Journal Article

Author(s):

Muhich, Christopher; Hoes, Marie; [Steinfeld, Aldo](#) 

Publication date:

2018-02-01

Permanent link:

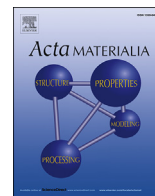
<https://doi.org/10.3929/ethz-b-000210450>

Rights / license:

[Creative Commons Attribution-NonCommercial-NoDerivatives 4.0 International](#)

Originally published in:

Acta Materialia 144, <https://doi.org/10.1016/j.actamat.2017.11.022>



Full length article

Mimicking tetravalent dopant behavior using paired charge compensating dopants to improve the redox performance of ceria for thermochemically splitting H₂O and CO₂

Christopher Muhich^{a, b, *}, Marie Hoes^a, Aldo Steinfeld^a^a ETH Zurich, Department of Mechanical and Process Engineering, 8092 Zurich, Switzerland^b Arizona State University, School for the Engineering of Matter, Transport and Energy, Tempe Arizona 85287, USA

ARTICLE INFO

Article history:

Received 17 August 2017

Received in revised form

16 October 2017

Accepted 11 November 2017

Available online 15 November 2017

Keywords:

Solar energy

Defect engineering

Density functional theory

Redox catalysis

Ceria

ABSTRACT

A novel doping strategy based on paired charge compensating dopants is proposed to improve the solar thermochemical H₂O and CO₂ splitting performance of ceria. Density functional theory based *ab initio* calculations show that by co-doping trivalent and pentavalent cations into ceria the behavior of the trivalent dopant resembles that of tetravalent dopants. In this study, which investigated combinations of group IIIA and VA elements, it was found that the trivalent dopant identity has the largest effect on the reduction energy, while the pentavalent dopant only slightly modifies it. The trivalent dopant in these materials suppresses the reduction energy due to decreased ionic attraction of the trivalent cation and O²⁻ as compared to Ce⁴⁺ and O²⁻. We predict relative reducing capabilities in the following decreasing order: Hf-CeO₂ > ScX-CeO₂ > Zr-CeO₂ > YX-CeO₂ > LaX-CeO₂ > undoped CeO₂ (where X = V, Nb or Ta). Experimental thermogravimetric analysis confirms the computational predictions.

© 2017 Acta Materialia Inc. Published by Elsevier Ltd. This is an open access article under the CC BY-NC-ND license (<http://creativecommons.org/licenses/by-nc-nd/4.0/>).

1. Introduction

The solar splitting of H₂O and CO₂ via a thermochemical redox cycle has the potential of reaching high solar-to-fuel energy efficiencies because it utilizes the entire spectrum of concentrated solar energy to produce H₂ and CO, separately or simultaneously, and in any desired ratio [1–4]. This 2-step cycle is represented by the coupled redox reactions:



In the first solar-driven endothermic step (Eq. (1)), a metal oxide MO_x is thermally reduced to MO_{x-δ} and O₂ evolves. In the second exothermic step (Eq. (2)), H₂O or CO₂ re-oxidized the reduced metal

oxide while generating H₂ or CO, respectively. Of the many metal oxides [3,5–8] that have been investigated for this redox cycle, CeO₂ has emerged as the state-of-the-art material because of its rapid redox kinetics and high crystallographic stability [7,9,10]. During cycling, the CeO₂ bulk reduces and oxidizes via the formation and annihilation of O-vacancy rather than complete material decomposition [9], which explains its stability over multiple cycles. However, bulk CeO₂, which is the relevant state for thermochemical cycling, exhibits low O-exchange capacities unless the reduction reaction is carried out at very high temperatures and low O₂ partial pressures, for example a non-stoichiometry of only 0.06 is achieved at 1773 K and an O₂ partial pressure 10⁻⁶ atm [11].

In an attempt to increase the production capacity of ceria, a wide array of dopants have been introduced into its lattice [3,7,12–16]. Of these, only Zr, Hf, and Sn have been shown to significantly improve the redox performance [12–14,17–19], although other cations increase kinetics or decrease grain growth, or are radioactive [15,16]. In order to facilitate the redox cycle, the dopants need to decrease the O-vacancy formation energy slightly while still being endothermic enough to favor the splitting of H₂O and CO₂, i.e. the reduction enthalpy ΔH_{red} must be at least 242 kJ/mol and 284 kJ/mol to split H₂O and CO₂, respectively [20]. The presence of Zr or Hf cations suppresses the O-vacancy formation energy enough to

* Corresponding author. Arizona State University, School for the Engineering of Matter, Transport and Energy, Tempe Arizona 85287, USA.

E-mail address: cmuhich@asu.edu (C. Muhich).

improve reduction while still enabling re-oxidation [21,22]. We recently showed that Zr and Hf doped ceria (Zr-CeO₂ and Hf-CeO₂) decrease the O-vacancy formation energy by storing strain energy in elongated O-Zr or O-Hf bonds which is released upon reduction and thereby compensates for O removal [23].

Conversely, the reduction of divalent and trivalent doped ceria is exothermic while pentavalent dopants and Ti are so small that they inherently break bond. The effects of divalent and trivalent dopant have been well studied, and cause the reduction reaction to be exothermic because of the under reduction of the O anions. Therefore, the removal of some O anions enables the reduction of the remaining O anions to their desired –2 oxidation state which is energetically favorable [24,25]. In these cases the reduction energy is below that required to split H₂O and CO₂, 242 kJ/mol and 284 kJ/mol respectively.

The presence of Sn changes the active mechanism, where CeO₂ and SnO₂ react to form a new pyrochlore (Ce₂Sn₂O₇) phase upon reduction that re-oxidizes to separate CeO₂ and SnO₂ phases during reduction. This phase change also occurs for Zr doped Ceria at very high temperatures and low oxygen partial pressure [26], however, the conditions necessary for these transitions are beyond those likely to be achievable during solar thermochemical water and carbon dioxide splitting [11,21,22]. Therefore, we restrict ourselves to O-vacancy mechanisms to avoid the sintering and slow kinetics problems often associated with phase change based processes.

In order to promote the two-step solar thermochemical redox cycle, the dopants must be tetravalent or have a higher oxidation state, be large enough to not inherently break bonds, and be less redox active than the Ce cations in the material. If new materials are to be developed that improve upon Zr- and Hf-CeO₂, elements from outside of group IVA need to be considered. While such elements exist which are tetravalent or higher, they are either too small or are redox active and thus have low reduction energies or initiate phase changes upon reduction [17,27]. Therefore a new doping paradigm is needed to make non-tetravalent dopants behave like tetravalent dopants while still meeting the other afore mentioned criteria. Additionally, it is desirable for the doped material to have a reduction energy between that of pure ceria and Zr-CeO₂ and Hf-CeO₂, as this will enable reduction at lower temperatures than CeO₂ and higher re-oxidation conversion extents than Zr- or Hf-CeO₂ [22].

In this work, we propose a novel modification strategy based on paired charge compensating doped (PCCD) ceria, where trivalent and pentavalent elements are co-doped into the host ceria lattice. By co-doping, the pentavalent cations cause the trivalent cations to behave like tetravalent cations. We use density functional theory based quantum simulations to show that the formation of O-vacancies at sites neighboring the trivalent dopant are sufficiently endothermic to drive water and carbon dioxide splitting and that the reduction energy is tunable via the selection of the trivalent species. Additionally, the reduction energies of PCCD-CeO₂ is between that of Zr-CeO₂ and undoped CeO₂, as is desired for improved redox performance. Thermogravimetric analysis of fabricated PCCD-CeO₂ materials verifies that they have the same relative reduction extents as the computational predictions, thus validating the computational results and analysis. This work opens up a new class of ceria materials which could be useful in many ceria based applications beyond just solar thermochemical fuels.

2. Methods

2.1. Computational methods

Period boundary condition density functional theory as implemented in the Quantum Espresso software package [28] was used

to investigate trivalent/pentavalent PCCD-CeO₂. The Perdew-Burke-Ernzerhof (PBE) [29] formulation of the generalized gradient approximation (GGA) was used to calculate the electronic exchange and correlation energies. The PBE functional was chosen as it gives similar results to the much more expensive HSE06 hybrid functional [30]. Ultra-soft pseudo-potentials [31] were used, enabling the exclusion of core electrons from the calculations. For the O ions, the 2s and 2p electrons were explicitly calculated. For all metallic elements, semi-core pseudopotential formulations were employed that included the highest energy s and p electrons of the core electrons in addition to the valence electrons. For example, the Ce ions included the 5s, and 5p, 6s, 5d, and 4f electrons. The wavefunction was composed of a summation of plane-waves with energies up to 530.6 eV (39 Ry). A cut-off energy study showed that there was only a 0.002 eV difference in the O-vacancy formation energy in undoped CeO₂ between a simulation with a 530.6 eV cut-off energy a 680.3 eV cut-off energy. The Brillion zone was sampled at the gamma point. Density of states (DOS) and partial densities of states (PDOS) were calculated on a 2 × 2 × 2 Monkhorst-Pack k-point mesh or finer.

In order to correct for the delocalization of Ce 4f bands, a 3.125 eV Hubbard [32] correction (DFT + U) was applied to Ce-f orbitals. This value represents a good compromise between electronic accuracy (i.e. two localized Ce 4f states in reduced CeO₂) and minimizing the depression of the calculated reduction energy for the pseudopotentials used [30]. No Hubbard correction was applied to the dopants as they do not, or only minimally, contribute to the f-band of the systems, and therefore their correction does not significantly affect reduction behavior [23].

A supercell composed of a 3 × 3 × 3 repetition of the primitive ceria fluorite cell was used to represent the material. This cell contains 27 cerium and 54 oxygen ions, and was chosen to represent likely reduction extents, and doping concentrations. Only bulk phase behavior was investigated, in other words there are no surfaces in the cell. Because of its large size (lattice vectors of ~11.5 Å) periodic image interactions are minimized. The formation of an oxygen vacancy in the supercell is equivalent to a reduction extent of $\delta = 0.037$ or a 1.85% O-vacancy concentration. For calculations of doped ceria, two cerium ions were replaced by dopant atoms – e.g. two Hf ions or one La and one Nb ion, which enabled the comparison of O-vacancy formation energies at equal dopant concentrations. The replacement of two cerium ions results in a dopant concentration of 7.4%.

O-vacancy formation energies were calculated using:

$$E_{\text{Ovac}} = E_{\text{MO}_{2-\delta}} + \frac{1}{2}E_{\text{O}_2} - E_{\text{MO}_2} \quad (3)$$

where E_{Ovac} is the O-vacancy formation energy (reduction energy), $E_{\text{MO}_{2-\delta}}$ is the energy of the supercell with an O-vacancy, E_{MO_2} is the energy of the supercell without a vacancy, and E_{O_2} is the energy of a gas phase O₂ molecule. Images showing the ionic configurations were generated using VESTA [33]. Charge analysis of the ions was conducted using the Bader method as implemented by the Henkelman group [34,35]. Like all charge assignment methods Bader analysis is a guide rather than a definitive determination of oxidation states.

The analysis performed here only considers the reduction energy and neglects entropic effects. This is because entropic effects are notoriously difficult to calculate accurately, which is exacerbated here due to the many possible configurations, and the associated configurational entropy and vibration entropy contributions at all possible geometric configurations. We therefore assume that the introduction of the dopants has only minor changes on the entropy of reduction, which enables us to compare reduction

behavior under identical conditions between similar materials. Previous work has suggested that this assumption is good when the materials are similar [20].

2.2. Experimental methods

2.2.1. Synthesis and sample characterization

Powders of $\text{Ce}_{0.9}\text{La}_{0.05}\text{Nb}_{0.05}\text{O}_2$ (LaNb5-CeO₂), $\text{Ce}_{0.9}\text{Y}_{0.05}\text{Nb}_{0.05}\text{O}_2$ (YNb5-CeO₂), $\text{Ce}_{0.9}\text{Sc}_{0.05}\text{Nb}_{0.05}\text{O}_2$ (ScNb5-CeO₂) and $\text{Ce}_{0.9}\text{Hf}_{0.1}\text{O}_2$ (Hf10-CeO₂) were produced according to a modified Pechini method as described by Meng et al. [18] Note that slightly different notation is used to ease differentiation between computational and experimental results. Citric acid (Sigma-Aldrich, 99%) in a molar ratio of 3:2 citric acid to metal cation was dissolved in 50 ml of anhydrous ethylene glycol (Sigma-Aldrich, 99.8%). In the case of Hf10-CeO₂, it was dissolved in 50 ml of deionized water. The respective metal cation nitrates and chlorides, namely cerium(III) nitrate hexahydrate (Sigma-Aldrich, 99%), Lanthanum(III) nitrate hexahydrate (Alfa Aesar, 99.9%), Yttrium(III) nitrate hexahydrate (Strem, 99.5%), Scandium(III) nitrate pentahydrate (Strem, 99.5%), Niobium(V) chloride (Strem, 99%) and Hafnium(IV) chloride (Alfa Aesar, 98%) were successively added to the ethylene glycol. The mixture was stirred for 2 h at 363 K on a magnetic hotplate. Then, the temperature was gradually increased until the ethylene glycol auto ignited and a powder was formed. The powders were calcined at 1273 K for 1 h. After cooling, the powder was uniaxially cold-pressed under 5 tons into dense cylindrical pellets with a diameter of 8 mm and masses ranging between 220 and 373 mg. Subsequently, the pellets were sintered at 1773 K for 5 h using a heating rate of 5 K/min.

2.2.2. Thermogravimetric analysis

Relative reduction extents of the various materials were measured based on their relative mass losses in a thermogravimetric analyzer (TGA, Setaram Setsys Evolution) at elevated temperatures and reduced O₂ partial pressures. The samples were suspended from the balance with a custom-made platinum hook to minimize mass transfer limitations between the sample and the surrounding gas atmosphere. The gas atmosphere in the TGA was controlled by varying the gas flow rates of Ar (Messer, 4.6) and O₂/

Ar (0.5 mol% O₂ in Ar, Messer, 5.0). Gas flows were adjusted using electronic mass flow controllers (Brooks, Model 5850TR, accuracy ± 1). A blank run (Al₂O₃ pellet) conducted under the same conditions was subtracted from the sample measurements to account for buoyancy effects. TGA experiments were conducted at $T = 1623$ K with a heating rate of 10 K/min and an oxygen partial pressure range of $p_{\text{O}_2} = 2.5 \times 10^{-4} - 4.75 \times 10^{-3}$ atm. The material was initially heated to 1073 K at $p_{\text{O}_2} = 4.75 \times 10^{-3}$ atm and allowed to equilibrate. Subsequently, the sample was heated to 1623 K followed by isothermal reduction and oxidation by rapidly changing the p_{O_2} and then allowing the system to reach equilibrium.

The relative mass loss of a sample is calculated according to:

$$\text{mass loss} = \frac{\Delta m}{m_{\text{sample}}} * 100\% \quad (4)$$

where Δm is the weight loss at equilibrium measured by the TGA, and m_{sample} is the sample mass.

3. Results and discussion

Here we will report on the O-vacancy formation energy of trivalent/pentavalent paired charge compensating dopants. The O-vacancy formation energy is used as the descriptor for redox activity, where O-vacancy formation energies higher than ceria are expected to perform poorly due to an inability to reduce at reasonable (<1773 K) temperatures, and low O-vacancy formation energies correspond to poor performance due to an inability to drive the water splitting reaction [20,23]. We first describe YNb-CeO₂ and compare its behavior to undoped ceria. We then describe the remaining PCCD combinations. We also compare the results to singly doped ceria to show that the PCCD effect is synergistic rather than an averaging of the reduction energies. Because this is the first report - to the best of our knowledge - of this ceria doping strategy, we confine the PCCD combinations to group IIIA and VA elements. Additionally, we restrict the discussion to the thermodynamics of reduction, leaving surface reactions and diffusion effects to future work. All calculations were conducted in bulk ceria, and the super cell remained neutrally charged for all configurations. Lastly, we present experimental relative reduction extents of select materials

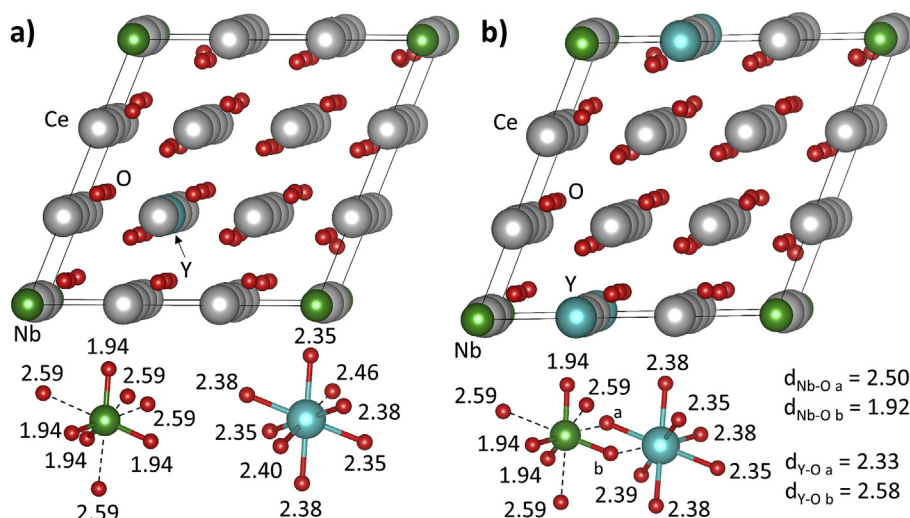


Fig. 1. Geometric representations of the a) 3NN_{Ce} and b) 1NN_{Ce} configuration of YNb-CeO₂. The black lines of the top figures indicate the bounds of the supercell. The lower configurations illustrate the coordination of the Y and Nb dopant cations. Large gray, large blue, medium green and small red spheres represent Ce, Y, Nb and O ions respectively. Numbers indicate interatomic distances in Angstroms (Å). In b), a and b are used to differentiate the shared O anions for labeling the distances. (For interpretation of the references to colour in this figure legend, the reader is referred to the web version of this article.)

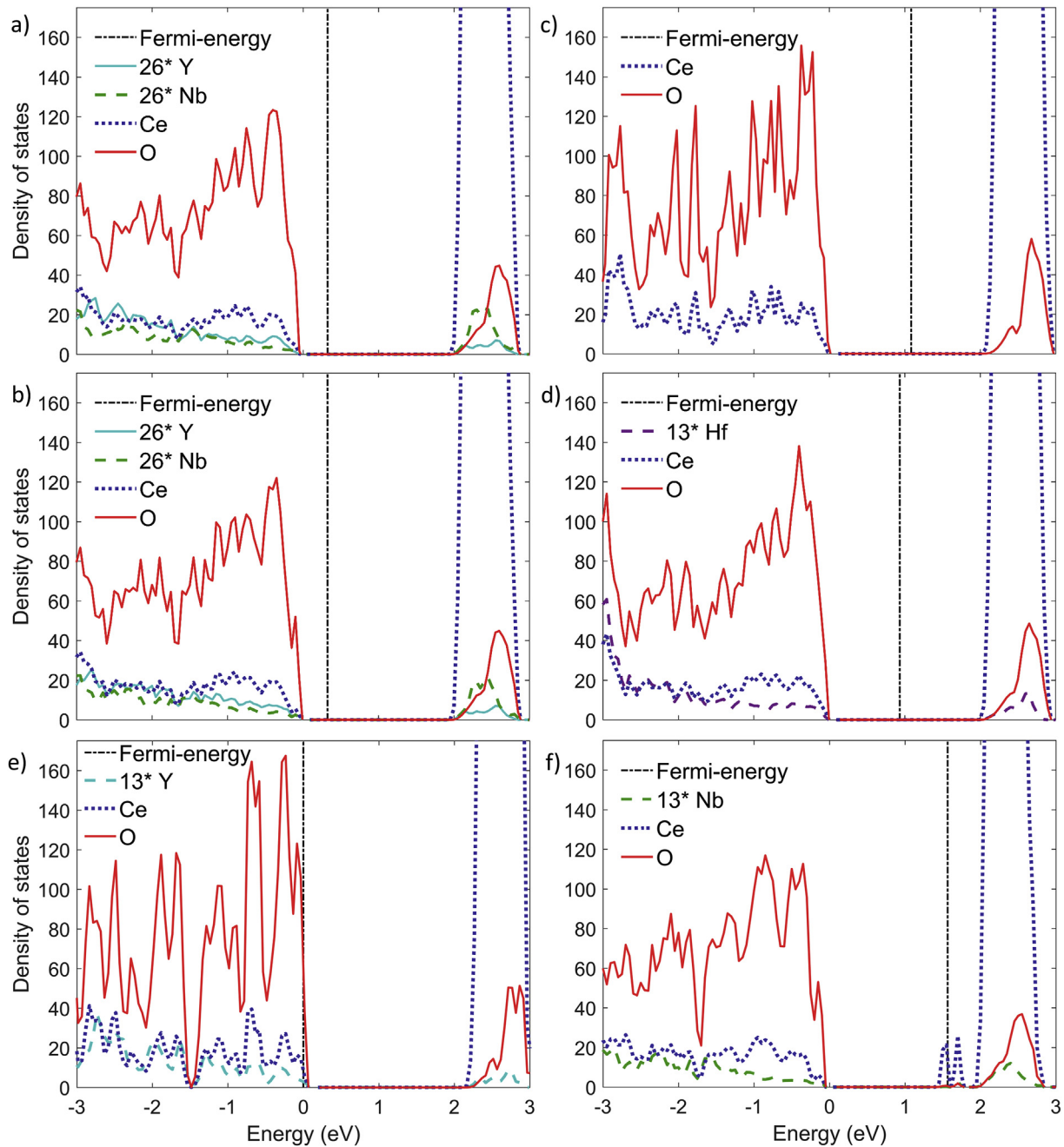


Fig. 2. Partial density of states plots of oxidized a) 3NN_{cc} YNb-CeO₂, b) 1NN_{cc} YNb-CeO₂, c) undoped CeO₂, d) Hf-CeO₂ e) Y-CeO₂ f) Nb-CeO₂. The PDOS plots are truncated to emphasize the details near the edges of the Valance and f-bands. The PDOS's of dopant cations have been increased to ease comparisons.

which agree with the computational predictions. In depth materials characterization is left to a separate work.

3.1. Oxidized YNb doped CeO₂

Ceria adopts the fluorite structure where the Ce cations are eightfold (cubically) coordinated, and the O anions are tetrahedrally coordinated. Introducing two dopants into the ceria lattice breaks the cationic and anionic symmetry, generating many unique sites. Therefore, we investigated two cationic configurations, and three O-vacancy sites. The cations were either third nearest cationic neighbors (~ 6.7 Å apart) which we call 3NN_{cc}, or were first nearest cationic neighbors (~ 3.8 Å apart) which we call 1NN_{cc}. These

configurations are exemplified by YNb-CeO₂ in Fig. 1. There is almost no thermodynamic preference for one cationic configuration of YNb-CeO₂ over the other (<0.006 eV preference for the 3NN_{cc} configuration which is well within the accuracy of the methods). Because there is no preference for pairing, the dopants are likely to be randomly distributed across cationic sites, suggesting that the number of 1NN_{cc} sites only depends on the doping concentrations and chance.

The electronic structure of PCCD-CeO₂ is generally similar to that of undoped ceria and tetravalent Hf-CeO₂. The partial density of states (PDOS) of fully oxidized YNb-CeO₂ shows a fully occupied valence band, i.e. no empty O 2p states, and empty Ce-f and conduction bands, where the Fermi level is within the band gap just

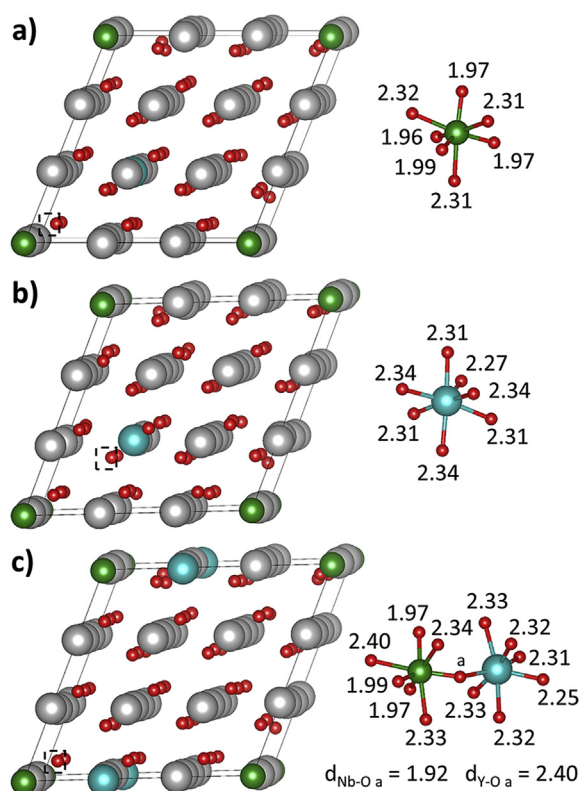


Fig. 3. Visualization of the reduced YNb-CeO₂ super cell showing a) 3NN_{O-5+}, b) 3NN_{O-3+}, and c) 1NN_{C-O-C} configurations. The left panel shows the entire super cell while the right panel details the coordination of the dopant cations neighboring the O-vacancy. Large gray, large blue, medium green and small red spheres represent Ce, Y, Nb and O ions respectively. The black dashed square shows the location of the vacancy. Numbers indicate interatomic distances in Angstroms (Å). The dopant-O distances for all attempted configurations are shown in SI Table S1-18. (For interpretation of the references to colour in this figure legend, the reader is referred to the web version of this article.)

like undoped CeO₂ and Hf-CeO₂, as shown in Fig. 2. This is in contrast to doping with only trivalent or pentavalent dopants, where the Fermi energy moves into the valence band, or new filled states appear, respectively, as shown in Fig. 2e and f. As in the case of Hf-CeO₂, some states associated with Y and Nb appear in the f-band; however, these comprise a small minority of the total. Nb states appear as a narrow band ~3.8 eV above the valence band maximum between the Ce f-band and the conduction band, which is composed primarily of Ce d-states, as shown in the supporting information (SI) Fig. S1. The PDOS's of all of the PCCD-CeO₂ materials are shown in SI Figs. S2–9. The “extra” electron of the pentavalent Nb cation, as compared to Ce, compensates for the “missing” electron of the trivalent Y cation, and thus all O anions are fully reduced. This behavior is different than either Y-CeO₂ or Nb-CeO₂, where the Fermi energy lies within the valence band or above a new state high in the valence band - f-band gap, respectively [23]. The PDOS analysis confirms the hypothesis that PCCDs behave like tetravalent dopants from an electronic perspective, and that reduction will require the promotion of two electrons to the conduction band.

There is one caveat to the tetravalent like behavior of the PCCDs, namely the charge on the dopant cations. In both cationic configurations, the Y dopant is less positively charged than the Ce cations or Hf cations in Hf-CeO₂, having Bader predicted charges of +2.14, +2.23, and +2.73 respectively, while the Nb dopants is more positively charged than Ce, with a +2.71 and + 2.68 charge in

the 3NN_{CC} and 1NN_{CC} configurations, respectively. The relative charges of Y and Nb as compared to Ce are unsurprising given that they are trivalent and pentavalent dopants.

The presence of Y and Nb dopants induces geometric changes in the ceria lattice. In both configurations the lattice vectors contract, from being symmetric and 11.67 Å long in pure ceria to being symmetric and 11.63 Å long in the 3NN_{CC} configuration and asymmetric with $a = b = 11.63$ Å and $c = 11.64$ Å in the 1NN_{CC} configuration. In addition to the contraction of the lattice, the local geometries also change. As in the case of Nb-CeO₂ and Y-CeO₂ [23], the Nb cation induces significant structural reconfiguration of its coordinating O anions in YNb-CeO₂ while Y does not. After relaxation in both 3NN_{CC} and 1NN_{CC} configurations, the Nb is tetrahedrally coordinated to four O anions with an average Nb-O bond length of 1.94 Å, while the remaining O anions have expanded to an average length of 2.57 Å. The 2.57 Å bond lengths suggest that four Nb-O bonds have been mostly severed, although ionic forces are still present, and that the O-anions are under-coordinated. The coordination of Y, conversely, remains mostly unchanged. In the 3NN_{CC} configuration, there is a slight distortion of the cubic configuration where four Y-O bonds have shrunk to 2.35 Å, three remain 2.38 Å long, and the O atom point towards the Nb cation is 2.45 Å away from the Y cation. In the 1NN_{CC} configuration, the bond lengths are more distorted, where Y-O bonds are 2.32–2.41 Å long, with the exception of one of the O anions shared with Nb, whose bond length has elongated to 2.58 Å. The configurations and bond lengths are detailed in Fig. 3. The long Y-O bond is associated with the O anion that is tetrahedral coordinated to the Nb atom, and therefore we attribute the long bond length to the effect of the Nb dopant rather than the Y. The presence of broken O-cation bonds neighboring the Nb dopants suggests that these sites will have substantially lowered O-vacancy formation energies compared to CeO₂. O anions that only neighbor the Y dopant, however, are expected to have only somewhat lowered reduction energies compared to CeO₂, due to decreased ionic interaction.

3.2. Reduction of YNb-CeO₂

We consider O-vacancy formation at three possible sites. When the cations are in the 3NN_{CC} configuration, O-vacancies were considered to occupy sites neighboring either the trivalent cation (3NN_{O-3+}) or the pentavalent cation (3NN_{O-5+}), as it has been shown that O-vacancies preferentially neighbor dopant cations [23]. In the 1NN_{CC} configuration the O-vacancy occupied sites neighboring both cations (1NN_{C-O-C}). The relaxed geometries of these sites are shown in Fig. 3. O-vacancy formation is endothermic by 1.97 eV, 2.51 eV and 1.69 eV for the 3NN_{O-5+}, 3NN_{O-3+}, and 1NN_{C-O-C} sites respectively. At all three sites the O-vacancy formation energy is substantially reduced from the 2.85 eV found in undoped ceria. The 3NN_{O-5+} and 3NN_{O-3+} sites, where the O-vacancies neighbor only one dopant are expected to be redox active because they store sufficient energy to split H₂O or CO₂; conversely, 1NN_{C-O-C} sites where the O-vacancy neighbors both Y and Nb do not store sufficient energy to abstract the O from H₂O or CO₂ and therefore are not expected to be redox active.

Upon reduction of YNb-CeO₂, two electrons worth of electron density are promoted into Ce f-states. This can be seen in Fig. 4a–c. These electrons form a new, narrow band that is slightly lower in energy and separate from the main Ce-f band and is composed of Ce 4f character. This indicates that Ce atoms are reducing rather than either of the dopants. This is logical as the Ce 4f states are lower in energy than the Nb or Y states. In the case of 3NN_{O-5+}, two new states appear in the bad gap, one that is filled and is associated with the promoted electrons and a second unfilled state. The high energy promotion of the two electrons from the valence band to Ce 4f

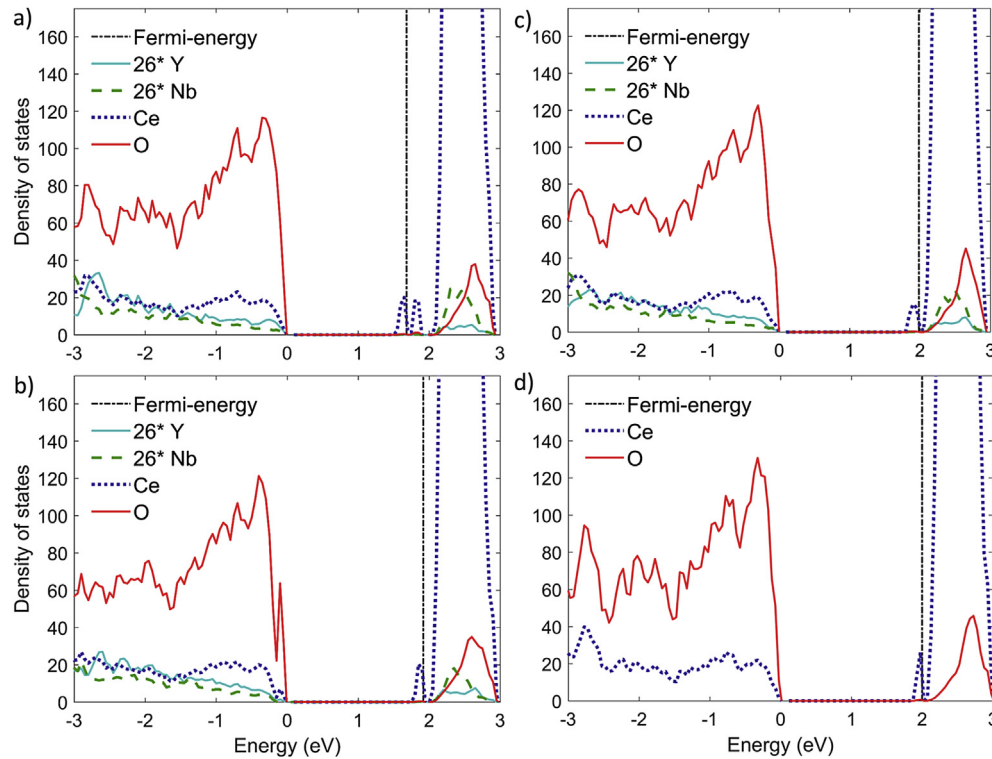


Fig. 4. Partial densities of state for reduced YNb-CeO₂ in the a) 3NN_{O-5+}, b) 3NN_{O-3+}, and c) 1NN_{C-O-C} configurations as well as d) undoped ceria for comparison. The PDOS plots are truncated to emphasize the details near the edges of the valance and f-bands. The PDOS's of dopant cations have been increased to ease comparisons.

states causes the reduction to be highly endothermic, similarly to what is seen for undoped ceria (Fig. 4d).

We attribute the decrease of the reduction energy of YNb-CeO₂ to broken O-Nb bonds, and decreased ionic bond strength of Y. The presence of Nb causes four O bonds to break, leaving four O anions under-coordinated. Therefore, generating an O-vacancy at the 3NN_{O-5+} site necessitates the breaking of only three O-cation bonds rather than the four of undoped ceria and thus the reduction energy is suppressed. At the 3NN_{O-3+} site no O-bonds are pre-broken, and thus O removal requires the severing of four O-cation bonds. This explains the higher O-vacancy formation energy at the 3NN_{O-3+} site as compared to 3NN_{O-5+} sites but does not explain the suppressed O-vacancy formation energy compared to undoped ceria. Because Y no longer behaves like a trivalent dopant, in the sense of causing an under-reduction of O anions, one might assume that Y cations decrease the O-vacancy formation energy by storing strain energy in the Y-O bonds which is released upon reduction, as is seen for Zr or Hf dopants [23]. However, this is not the case because the Y-O bond lengths before and after O removal (2.38 and 2.32 Å respectively, not including the extra elongated or contracted bond) closely match the Ce-O bond lengths in undoped ceria (2.38 and 2.33 Å respectively), as shown in Fig. 3. Therefore, any strain release would be minimal and be unable to account for the 0.34 eV decrease in reduction energy. We attribute the decreased O-vacancy formation energy to the relative strengths of the ionic interactions of Ce⁴⁺ and Y³⁺ with O²⁻. The Y cation is less oxidized than the Ce cations as shown by their Bader charges of +2.14 + 2.23, respectively; therefore, the ionic attraction of O²⁻ to Y³⁺ is weaker than to Ce⁴⁺ making O abstraction less endothermic.

The largest suppression of the O-vacancy formation energy is seen at the 1NN_{C-O-C} sites, and arises from the combined effects of both dopants. In fact, the summation of the decrease in reduction energies as compared to pure ceria at the 3NN_{O-3+} and 3NN_{O-5+}

sites (0.34 eV and 0.88 eV respectively for a 1.22 eV total effect) is roughly the same as the decrease in reduction energy found at the 1NN_{C-O-C} site (1.16 eV). Overall, this shows that the PCCD-CeO₂ offers a reduction energy that is expected to facilitate redox cycling and that co-doping results in a synergistic effect where the trivalent dopant acts more similarly to a tetravalent dopant than ceria doped with only trivalent dopants.

3.2.1. Effect of trivalent and pentavalent cation identity on the results

Eight other PCCD combinations were examined for their preferred cationic configurations and reduction behavior. For the remaining PCCD materials there is little to no driving force for the cations to pair (<0.1 eV). However, different combinations of trivalent and pentavalent dopants alter the reduction energies of ceria to varying extents as shown in Fig. 5a–c and Table 1. As in the case of YNb-CeO₂, the O-vacancy formation energy is site dependent with relative energies of 1NN_{C-O-C} < 3NN_{+5-O} < 3NN_{+3-O}. The identity of the trivalent dopant has the largest effect on the O-vacancy formation energy, except when the O-vacancy only neighbors the pentavalent dopant where all nine investigated combinations have roughly the same energy (within 0.18 eV of each other).

The trivalent dopant decreases the O-vacancy formation energy depending on their identity where PCCD materials have relative reduction energies of ScX-CeO₂ < YX-CeO₂ < LaX-CeO₂ (where X is V, Nb, or Ta) regardless of the pentavalent dopant. This arises due to their relative extents of oxidation. As described for YNb-CeO₂, the trivalent dopant suppresses the reduction energy by decreasing the ionic attraction between O²⁻ anions and the cations; therefore, less positive cations are expected to have lower O-vacancy formation energies than more positively charged cations. The effect of this is illustrated in Fig. 5d, where the O-vacancy formation energy is

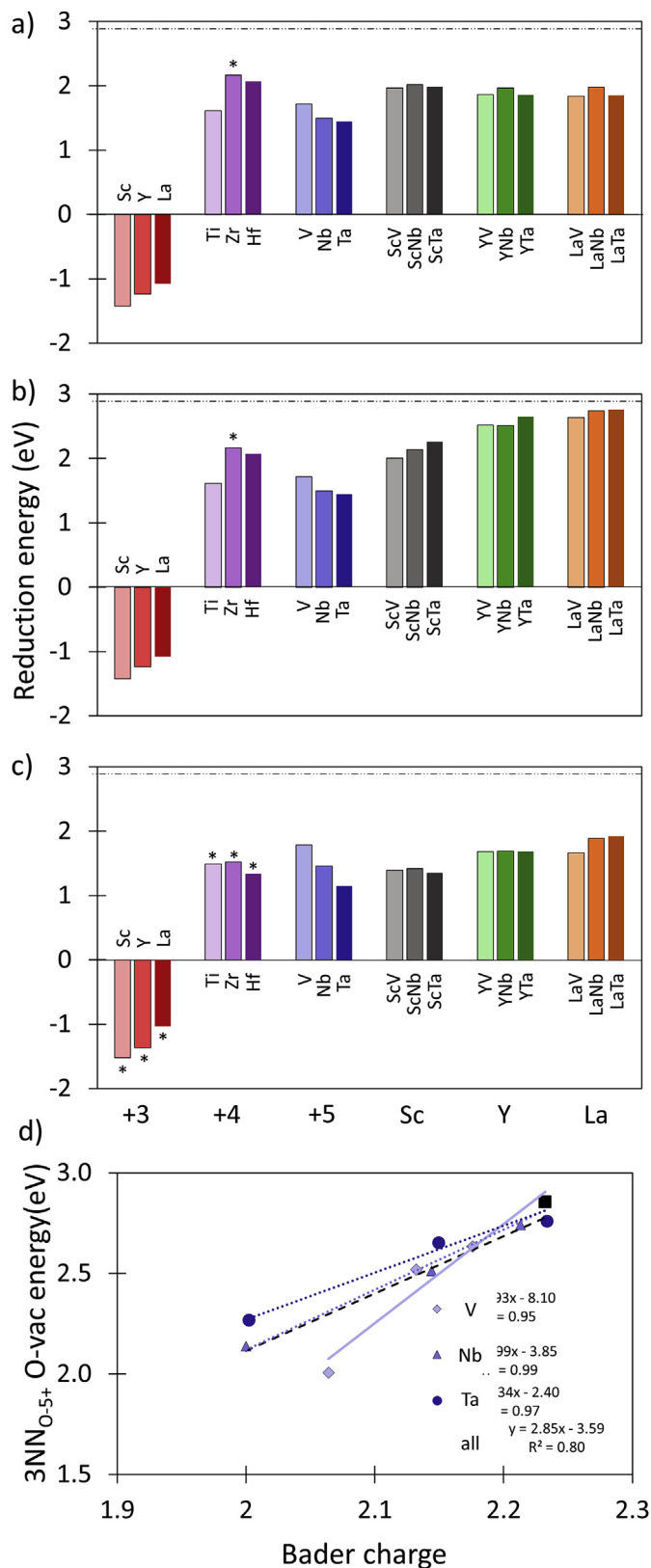


Fig. 5. Relative energies of reduction of doped ceria with a 7.4% doping concentration. The plots show the O-vacancy in the a) 3NN_{O-5+}, b) 3NN_{O-3+}, and c) 1NN_{Ce-O-Ce} configurations. For the purely tri-, tetra- and pentavalent dopants a) and b) show level as there is only one dopant cation. The reduction energy of undoped ceria is indicated by the dotted-dashed line at taken from Ref. [18]. d) shows the correlation between the charge of the trivalent cation in PCCD-ceria and the charge of the reduction energy. The black square represents a Ce cation in undoped CeO₂, the black dashed line represents the linear regression of the whole data set.

plotted against the Bader charge. The good linear correlation between the Bader charge of the trivalent cation and O-vacancy formation energy suggests that the ionic attraction explanation is reasonable because ionic interactions scale linearly with charge. While this correlation is best when comparisons are made between PCCD's with the same pentavalent dopant ($R^2 = 0.83$, >0.99 , >0.99 for V, Nb and Ta respectively when including Ce in undoped ceria as a data point in the fit), the correlation is still good when all combinations are considered ($R^2 = 0.81$). The fact that undoped ceria was included in the fitting that resulted in a good correlation further bolsters the attraction explanation because this suggests that secondary effects like strain or different bonding mechanisms are not the main effect (see SI Fig. S10 for a comparison of Bader charge and reduction energy for ceria doped singly with tetravalent and pentavalent dopants).

When there is an O-vacancy in the 3NN_{O-5+} configuration, there is a maximum difference in reduction energies of 0.17 eV, which is significantly smaller than the 0.75 eV range at a 3NN_{O-5+}. The pentavalent dopants have a smaller effect because they are more similar to each other than the trivalent dopants. The pentavalent dopants all induce massive structural re-arrangement due to their smaller ionic radii (V-0.68 Å, Nb-0.78 Å, and Ta-0.78 Å) than Ce (1.01 Å) which results in broken O bonds. Because the presence of broken O-bonds is the main cause of O-vacancy formation energy reduction for pentavalent dopants and all three pentavalent elements break bonds, it is unsurprising that they behave similarly. Density of states plots and super-cell geometric information for all PCCD-CeO₂ are contained in SI Figures S2-S9 and SI Tables S1-S9.

3.3. Single element doped ceria

The reduction energies and configurational preference energies were calculated for ceria doped with only a single element in the same configurations described for the PCCD materials. The results are summarized in Table 1. Here we just point out major trends. For more detailed analysis of the effects of singly doped ceria see Muhich and Steinfeld [23]. The dopants decrease the reduction energy of ceria with relative energies of trivalent (single vacancy) $< 0 <$ pentavalent $<$ tetravalent undoped, as shown in Fig. 5. The reduction of trivalent doped ceria is exothermic, while tetra- and pentavalent dopants are endothermic. When a second O-vacancy is introduced into the trivalent cation doped ceria, the O-vacancy formation energy becomes endothermic and roughly equal to that of undoped ceria because two electrons must once again be promoted to the high energy Ce-f band [25]. This is because the trivalent dopants cause the under reduction of the O anions and, therefore, the reduction does not require the promotion of electrons into the Ce-f band, the pentavalent dopants break O bonds, and the tetravalent dopants only strain the O bonds. For all of the dopants investigated, the O-vacancy formation energy is lowest when the vacancy occupies a site neighboring two dopants, because the effects are cumulative, but the effect is largest for Zr- and Hf-CeO₂. The relative energies of the single element doped materials are all lower than the PCCD-CeO₂, except Sc based PCCD materials which have reduction energies between Zr- and Hf-CeO₂.

The relative energies of the two cation configurations depend on the identity of the dopant. The pentavalent, and Ti and Sc dopants attract each other, while the remaining tetra- and trivalent dopants do not. This suggests that while Y, La, Zr and Hf will be randomly distributed through the lattice, the other dopants form pairs.

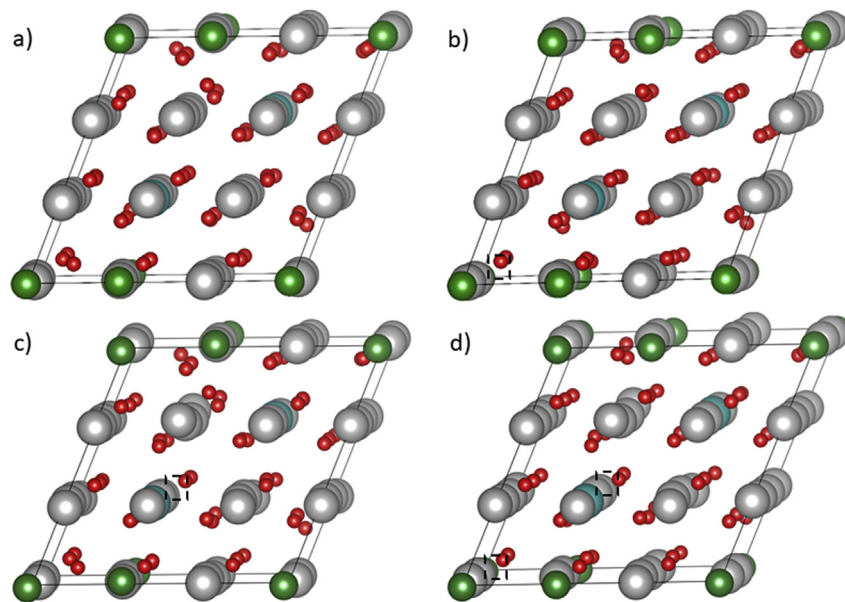
3.4. Expected structures and reduction behavior of doped ceria

In order to predict the redox behavior of PCCD-CeO₂ materials it is necessary to understand both the available structures and their

Table 1

Summary of computational energetic and Bader charge results.

1NNcc preference (eV) ^a			3NN _{cc} Bader charge		1NNcc Bader charge		Reduction energy (eV)		
			+5	+3	+5	+3	3NN _{cc} -5+	3NN _{cc} -3+	1NN _{cc} -o-c
ScX	CeO ₂	n/a	2.23 ^b				2.85 ^b		
	Sc v	0.00	2.11	2.06	2.10	2.07	1.97	2.01	1.40
	Sc Nb	−0.04	2.71	2.00	2.70	2.06	2.02	2.14	1.42
YX	Sc ta	−0.03	2.88	2.00	2.86	2.03	1.98	2.27	1.35
	Y v	0.00	2.07	2.13	2.07	2.10	1.86	2.52	1.68
	Y Nb	0.01	2.71	2.14	2.71	2.15	1.97	2.51	1.69
LaX	Y Ta	0.00	2.87	2.15	2.83	2.17	1.86	2.65	1.68
	La V	−0.08	2.07	2.18	2.07	2.18	1.84	2.64	1.67
	La Nb	−0.06	2.70	2.21	2.68	2.21	1.98	2.74	1.89
+3	La Ta	−0.07	2.86	2.23	2.83	2.21	1.85	2.76	1.92
	Sc	−0.44		2.02		2.06		−1.42	−1.52
	Y	−0.06		2.02		2.06		−1.24	−1.37
+4	La	−0.03		2.24		2.25		−1.07	−1.03
	Ti	−0.73	2.12 ^b		2.09 ^b		1.61 ^b		1.49
	Zr	0.01	2.39 ^b		2.48 ^b		2.17 ^b		1.52
+5	Hf	0.03	2.74 ^b		2.64 ^b		2.07 ^b		1.34
	V	−1.23	2.08/2.11 ^c		2.08/2.11 ^c		1.72		1.79
	Nb	−0.63	2.58		2.59		1.50		1.46
	Ta	−0.48	2.85		2.83		1.45		1.15

^a The energy difference between the 1NN_{cc} and 3NN_{cc} configurations, a negative energy indicates that the 1NN_{cc} configuration is preferred.^b The formally tetravalent cations are grouped with the pentavalent cations for space reasons.^c The V cations do not have equal charge and therefore the charge of each cation is shown.**Fig. 6.** Visualization of the high concentration YNb-Ce-O₂ super cell showing a) the oxidized state, singly reduced with a vacancy at the b) 1NN₅₊-O-5+ and c) 3NN₀₋₃₊ sites, and d) the doubly reduced cell with vacancies in both 1NN₅₊-O-5+ and 3NN₀₋₃₊ sites. Large gray, large blue, medium green and small red spheres represent Ce, Y, Nb and O ions respectively. The black dashed square shows the location of the vacancy. (For interpretation of the references to colour in this figure legend, the reader is referred to the web version of this article.)

relative O-vacancy formation energy and thereby their reduction behavior. Therefore, we first discuss the structures that are available, the relative reducibility of the structure and finally the predicted impact of PCCD on the redox behavior of ceria.

3.4.1. Structures of PCCD ceria

O-vacancy formation at the three dopant neighboring sites (1NN_{c-o-c}, 3NN₊₅₋₀, 3NN₊₃₋₀) differs based on the identity of the coordinating cations; however, which O coordination structures are available is a more complex matter. As mentioned in the results section, the PCCD and trivalent dopants (except Sc) are expected to be randomly distributed throughout the material due to the low or

unfavorable pairing energy (<0.1 eV), while the pentavalent dopants have a strong driving force for pairing (>0.46 eV). Therefore, we predict that the pentavalent dopants in PCCD ceria will form pairs, leaving the trivalent dopants randomly distributed on the lattice. This leaves O sites that neighbor two pentavalent dopants, and sites that neighbor trivalent dopants. Additionally, there will be some O sites which neighbor multiple trivalent dopants as the dopants are randomly distributed. However, we assume low concentrations of dopants and therefore consider the trivalent dopants to be unpaired.

Based on the energies of the configurations considered in Section 3.3 and 3.4 and the analysis given above, i.e. the doped material

contains isolated trivalent dopants and paired pentavalent dopants, we do not expect O sites in all of these configurations to be redox active. Rather we first expect low energy O-vacancies to form at the $1\text{NN}_{5+-0-5+}$ sites which are not H_2O or CO_2 splitting redox active; subsequently, we expect high energy O-vacancies to form at 3NN_{+3-0} sites which are redox active. To test this, we constructed a super cell containing two separated Y^{3+} cations and two neighboring Nb^{5+} cations, and removed two O anions, as shown in Fig. 6. We calculate that an O-vacancy forms at the $1\text{NN}_{5+-0-5+}$ site with a reduction energy of 1.75 eV, which is lower than when the O-vacancy neighbors a Y^{3+} dopant (2.42 eV). These sites are shown in Fig. 6. The ordering of the vacancy site preferences is consistent with the energies calculated in super cells containing only two dopants (or no dopants) with similar configurations, and the energy are only slightly altered, where the 1NN_{+3-0} site is slightly stabilized and the $1\text{NN}_{5+-0-5+}$ site is slightly destabilized. We attribute these changes to the increased dopant concentration. Once again we suggest that the $1\text{NN}_{5+-0-5+}$ site does not store sufficient energy to abstract an O from H_2O or CO_2 and therefore this site is not gas splitting redox active. Because of the strong site preference for the first vacancy, we consider that an O-vacancy occupies the $1\text{NN}_{5+-0-5+}$ site when the second vacancy forms. We calculate that the second vacancy has a formation energy of 2.33 eV when it occupies a 3NN_{+3-0} site. The reduction energy of the active 3NN_{+3-0} site in the high dopant concentration super cell (2.42 eV and 2.33 eV for the first and second O-vacancy) is similar to that of the lower concentration YNb-CeO_2 super cell (2.51 eV). Additionally, these reduction energies have not changed sufficiently to alter the relative ordering of the reduction energies of the PCCD materials. This suggests that the lower dopant concentration super cell without an O-vacancy neighboring the pentavalent dopant is a good representative model for the more complicated system tested here. Therefore, we consider only the configurations with one set of PCCD for the rest of our analysis.

Because of its low O-vacancy formation energy, O vacancies are likely to form at the O-sites neighboring two pentavalent dopants even at moderate temperatures and slightly reduced O_2 partial pressures. However, because the reduction energy at these sites is so low that insufficient energy is stored in the vacancy to abstract an O atom from water or carbon dioxide, and therefore these sites are considered to be inactive for solar thermochemical water or carbon dioxide splitting. The isolated trivalent sites, however, have reduction energies that are substantially higher, although lower than undoped ceria. We predict that the 3NN_{0-3+} sites are the H_2O and CO_2 splitting active sites, and thus that the O-vacancy formation energy for these sites should be used for predicting redox behavior.

3.4.2. Predicted reducibility of PCCD- CeO_2

Based on the O-vacancy formation energies detailed in Table 1 and Fig. 5, we can predict the relative reduction extents, and therefore mass losses, of doped ceria at intermediate to high temperatures. With the understanding that we expect the pentavalent dopants to pair, leaving isolated trivalent dopants, we use the 3NN_{0-3+} O-vacancy formation energies for the predictions. The relative reduction extents for Nb based PCCDs are predicted to be $\text{ScNb-CeO}_2 > \text{YNb-CeO}_2 > \text{LaNb-CeO}_2$ at a given O_2 partial pressure and temperature. We only list the Nb based PCCDs because the identity of the pentavalent dopant is predicted to have a minimal effect and does not alter the ordering above. Additionally, YNb and LaNb PCCD materials are expected to have reduction energies between that of Zr doped ceria and pure ceria while ScNb behavior is expected to lie between Zr and Hf doped ceria giving a predicted relative reducibility of $\text{Hf-CeO}_2 > \text{ScNb-CeO}_2 > \text{Zr-CeO}_2 > \text{YNb-CeO}_2 > \text{LaNb-CeO}_2 > \text{pure ceria}$.

3.5. Experimental relative reduction extents of PCCD materials

The relative reduction extents of Nb based PCCD- CeO_2 , Hf doped ceria and pure ceria were determined by their mass losses at high temperatures and low O_2 partial pressures as measured via thermogravimetric analysis. The samples were reduced at 1623 K under several low O_2 partial pressures. The resulting mass losses are displayed in Fig. 7. The mass loss is attributed to reduction and O_2 generation because it is reversible upon exposure to higher O_2 partial pressures. Upon heating, the materials began to reduce and at the final temperature the materials exhibited relative mass losses of $\text{Hf} > \text{ScNb} > \text{YNb} > \text{LaNb} > \text{pure ceria}$. The order remained the same regardless of the oxygen partial pressure, although at lower oxygen partial pressures the mass losses were higher. Further and more in depth experimental analysis and materials characterization can be found in Hoes et al. [36]. These experimentally determined relative reduction extents match the computationally predicted behavior. This suggests that the computational results and the associated analysis is likely correct, and that PCCD- CeO_2 materials seem to be a way to extending the range of available ceria redox energies.

4. Conclusions

We have developed a novel dopant strategy based on paired charge compensating dopants to improve the redox performance of ceria. By co-doping tri- and pentavalent dopants, the material behaves as if it were doped with a tetravalent dopant but with an increased range of O-vacancy formation energies, which depends on the chosen trivalent dopant. Specifically, we investigated all possible trivalent and pentavalent combinations from the IIIA and VA groups and found that the trivalent dopant has a larger impact on the O-vacancy formation energy where less oxidized cations result in lower O-vacancy formation energies. Based on the computed reduction energies we predicted and experimentally verified that the PCCD materials reduce less than Hf doped ceria but more than undoped ceria, and that they have relative reduction

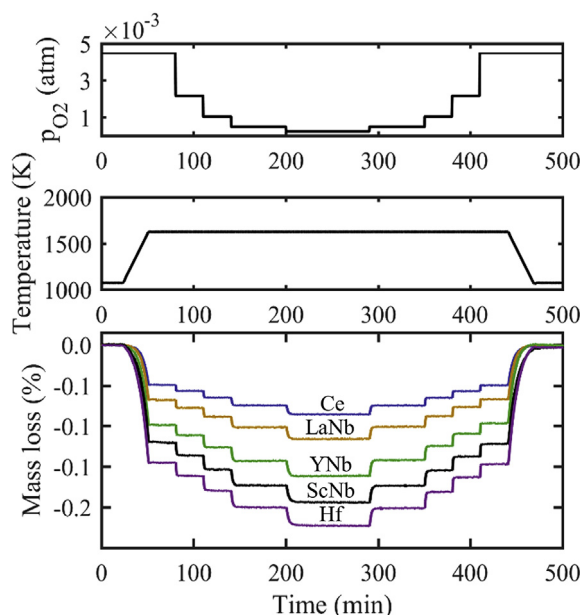


Fig. 7. Thermogravimetric analysis of PCCD- CeO_2 at 1623 K; both undoped ceria and Hf- CeO_2 are included for reference. The top, middle, and bottom plots displays, respectively, the O_2 partial pressure and temperature of the system, and resulting mass changes of the sample.

extents of: $\text{Hf} > \text{ScNb} > \text{YNb} > \text{LaNb} > \text{undoped ceria}$. Additionally, because the PCCD materials have larger reduction energies than Hf- and Zr-CeO₂, they are predicted to achieve higher re-oxidation conversion extents under identical solar thermochemical gas splitting oxidation conditions while still reducing more than pure ceria under identical reduction conditions.

While this work only investigated the IIIA/VA group dopants for PCCD-CeO₂ materials, there are many more combinations available owing to the large number of elements which adopt a 3 + oxidation state. Therefore, ample opportunities exist to develop more dopant combinations with a wider range of O-vacancy formation energies. In this work, the O-vacancy formation energies have been assessed in terms of the solar thermochemical splitting of H₂O and CO₂, where energies between Hf-doped and undoped ceria are of interest. However, the paired charge compensating doping strategy could be extended to other applications where ceria is used, such as catalytic converters and fuel cells/electrolyzes, where the O-vacancy energy needs to be tuned to provide optimal performance.

Acknowledgements

We gratefully acknowledge the financial support by the Swiss State Secretariat for Education, Research and Innovation, the EU's Horizon 2020 research and innovation program (SUN-to-LIQUID – No. 654408), and the European Research Council Advanced Grant (SUNFUELS – No. 320541). The DFT calculations were performed at the High-Performance Computation cluster of ETH Zürich.

Appendix A. Supplementary data

Supplementary data related to this article can be found at <https://doi.org/10.1016/j.actamat.2017.11.022>.

References

- [1] N.P. Siegel, J.E. Miller, I. Ermanoski, R.B. Diver, E.B. Stechel, Factors affecting the efficiency of solar driven metal oxide thermochemical cycles, *Industrial Eng. Chem. Res.* 52 (9) (2013) 3276–3286.
- [2] A. Steinfeld, Solar thermochemical production of hydrogen—a review, *Sol. Energy* 78 (5) (2005) 603–615.
- [3] C.L. Muhich, B.D. Ehrhart, I. Al-Shankiti, B.J. Ward, C.B. Musgrave, A.W. Weimer, A review and perspective of efficient hydrogen generation via solar thermal water splitting, *Wiley Interdisciplinary Reviews, Energy Environ.* 5 (3) (2016) 261–287.
- [4] P. Furler, J.R. Scheffe, A. Steinfeld, Syngas production by simultaneous splitting of H₂O and CO₂ via ceria redox reactions in a high-temperature solar reactor, *Energy & Environ. Sci.* 5 (3) (2012) 6098–6103.
- [5] N. Gokon, T. Mataga, N. Kondo, T. Kodama, Thermochemical two-step water splitting by internally circulating fluidized bed of NiFe₂O₄ particles: successive reaction of thermal-reduction and water-decomposition steps, *Int. J. Hydrogen Energy* 36 (8) (2011) 4757–4767.
- [6] M. Takacs, M. Hoes, M. Caduff, T. Cooper, J.R. Scheffe, A. Steinfeld, Oxygen nonstoichiometry, defect equilibria, and thermodynamic characterization of LaMnO₃ perovskites with Ca/Sr A-site and Al B-site doping, *Acta Mater.* 103 (2016) 700–710.
- [7] J.R. Scheffe, A. Steinfeld, Oxygen exchange materials for solar thermochemical splitting of H₂O and CO₂: a review, *Mater. Today* 17 (7) (2014) 341–348.
- [8] B. Meredig, C. Wolverton, First-principles thermodynamic framework for the evaluation of the thermochemical H₂O or CO₂ splitting materials, *Phys. Rev. B* 80 (24) (2009) 245119.
- [9] W.C. Chueh, S.M. Haile, A thermochemical study of ceria: exploiting an old material for new modes of energy conversion and CO₂ mitigation, *Philosophical Transactions of the Royal Society A: Mathematical, Phys. Eng. Sci.* 368 (1923) (2010) 3269–3294.
- [10] W.C. Chueh, C. Falter, M. Abbott, D. Scipio, P. Furler, S.M. Haile, A. Steinfeld, High-flux solar-driven thermochemical dissociation of CO₂ and H₂O using nonstoichiometric ceria, *Science* 330 (6012) (2010) 1797–1801.
- [11] R.J. Panlener, R.N. Blumenthal, J.E. Garnier, A thermodynamic study of non-stoichiometric cerium dioxide, *J. Phys. Chem. Solids* 36 (11) (1975) 1213–1222.
- [12] J.R. Scheffe, R. Jacot, G.R. Patzke, A. Steinfeld, Synthesis, characterization, and thermochemical redox performance of Hf⁴⁺, Zr⁴⁺, and Sc³⁺ doped ceria for splitting CO₂, *J. Phys. Chem. C* 117 (46) (2013) 24104–24114.
- [13] A. Le Gal, S. Abanades, G. Flamant, CO₂ and H₂O splitting for thermochemical production of solar fuels using nonstoichiometric ceria and ceria/zirconia solid solutions, *Energy & Fuels* 25 (10) (2011) 4836–4845.
- [14] B. Bulfin, F. Call, J. Vieten, M. Roeb, C. Sattler, I.V. Shvets, Oxidation and reduction reaction kinetics of mixed cerium zirconium oxides, *J. Phys. Chem. C* 120 (4) (2016) 2027–2035.
- [15] F. Call, M. Roeb, M. Schmücker, C. Sattler, R. Pitz-Paal, Ceria doped with zirconium and lanthanide oxides to enhance solar thermochemical production of fuels, *J. Phys. Chem. C* 119 (13) (2015) 6929–6938.
- [16] J. Scaranto, H. Idriss, The effect of uranium cations on the redox properties of CeO₂ within the context of hydrogen production from water, *Top. Catal.* 58 (2015) 143–148.
- [17] C. Ruan, Y. Tan, L. Li, J. Wang, X. Liu, X. Wang, A novel CeO₂–xSnO₂/Ce₂Sn₂O₇ pyrochlore cycle for enhanced solar thermochemical water splitting, *AIChE J.* 63 (8) (2017) 3450–3462.
- [18] Q.-L. Meng, C.-i. Lee, T. Ishihara, H. Kaneko, Y. Tamaura, Reactivity of CeO₂-based ceramics for solar hydrogen production via a two-step water-splitting cycle with concentrated solar energy, *Int. J. Hydrogen Energy* 36 (21) (2011) 13435–13441.
- [19] G. Balducci, M.S. Islam, J. Kašpar, P. Fornasiero, M. Graziani, Bulk reduction and oxygen migration in the ceria-based oxides, *Chem. Mater.* 12 (3) (2000) 677–681.
- [20] C.L. Muhich, B.D. Ehrhart, V.A. Witte, S.L. Miller, E.N. Coker, C.B. Musgrave, A.W. Weimer, Predicting the solar thermochemical water splitting ability and reaction mechanism of metal oxides: a case study of the hercynite family of water splitting cycles, *Energy & Environ. Sci.* 8 (12) (2015) 3687–3699.
- [21] B. Bulfin, L. Hoffmann, L. de Oliveira, N. Knoblauch, F. Call, M. Roeb, C. Sattler, M. Schmücker, Statistical thermodynamics of non-stoichiometric ceria and ceria zirconia solid solutions, *Phys. Chem. Chem. Phys.* 18 (33) (2016) 23147–23154.
- [22] M. Takacs, J.R. Scheffe, A. Steinfeld, Oxygen nonstoichiometry and thermodynamic characterization of Zr doped ceria in the 1573–1773 K temperature range, *Phys. Chem. Chem. Phys.* 17 (12) (2015) 7813–7822.
- [23] C.L. Muhich, A. Steinfeld, Principles of doping ceria for the solar thermochemical redox splitting of H₂O and CO₂, *J. Mater. Chem. A* 5 (30) (2017) 15578–15590.
- [24] T. Otake, H. Yugami, K. Yashiro, Y. Nigara, T. Kawada, J. Mizusaki, Non-stoichiometry of Ce_{1-x}Y_xO_{2-0.5x-δ} (X=0.1, 0.2), *Solid State Ionics* 161 (1–2) (2003) 181–186.
- [25] C. Muhich, A. Steinfeld, Principles of doping ceria for the solar thermochemical redox splitting of H₂O and CO₂, *J. Mater. Chem. A* 5 (30) (2017) 15578–15590.
- [26] T. Montini, N. Hickey, P. Fornasiero, M. Graziani, M.A. Banares, M.V. Martinez-Huerta, I. Alessandri, L.E. Depero, Variations in the extent of pyrochlore-type cation ordering in Ce₂Zr₂O₈: a t'–κ pathway to low-temperature reduction, *Chem. Mater.* 17 (5) (2005) 1157–1166.
- [27] D.A. Andersson, S. Simak, N.V. Skorodumova, I. Abrikosov, B. Johansson, Theoretical study of Ce O₂ doped with tetravalent ions, *Phys. Rev. B* 76 (17) (2007) 174119.
- [28] P. Giannozzi, S. Baroni, N. Bonini, M. Calandra, R. Car, C. Cavazzoni, D. Ceresoli, G.L. Chiarotti, M. Cococcioni, I. Dabo, A. Dal Corso, S. de Gironcoli, S. Fabris, G. Fratesi, R. Gebauer, U. Gerstmann, C. Gougousis, A. Kokalj, M. Lazzeri, L. Martin-Samos, N. Marzari, F. Mauri, R. Mazzarello, S. Paolini, A. Pasquarello, L. Paulatto, C. Sbraccia, S. Scandolo, G. Sclauzero, A.P. Seitsonen, A. Smogunov, P. Umari, R.M. Wentzcovitch, QUANTUM ESPRESSO: a modular and open-source software project for quantum simulations of materials, *J. Phys. Condens. Matter Inst. Phys. J.* 21 (39) (2009) 395502.
- [29] J.P. Perdew, K. Burke, M. Ernzerhof, Generalized gradient approximation made simple, *Phys. Rev. Lett.* 77 (18) (1996) 3865.
- [30] C.L. Muhich, Re-evaluating CeO₂ expansion upon reduction: non-counterpoised forces, not ionic radius effects, are the cause, *J. Phys. Chem. C* 121 (14) (2017) 8052–8059.
- [31] D. Vanderbilt, Soft self-consistent pseudopotentials in a generalized eigenvalue formalism, *Phys. Rev. B* 41 (11) (1990) 7892–7895.
- [32] J. Hubbard, Electron correlations in narrow energy bands, *Proc. R. Soc. Lond. Ser. A-Mathematical Phys. Sci.* 276 (1364) (1963) 238–257.
- [33] K. Momma, F. Izumi, VESTA 3 for three-dimensional visualization of crystal, volumetric and morphology data, *J. Appl. Crystallogr.* 44 (6) (2011) 1272–1276.
- [34] G. Henkelman, A. Arnaldsson, H. Jónsson, A fast and robust algorithm for Bader decomposition of charge density, *Comput. Mater. Sci.* 36 (3) (2006) 354–360.
- [35] E. Sanville, S.D. Kenny, R. Smith, G. Henkelman, Improved grid-based algorithm for Bader charge allocation, *J. Comput. Chem.* 28 (5) (2007) 899–908.
- [36] M. Hoes, C.L. Muhich, R. Jacot, G.R. Patzke, A. Steinfeld, Thermodynamics of paired charge-compensating doped ceria with superior redox performance for solar thermochemical splitting of H₂O and CO₂, *J. Mater. Chem. A* (5) (2017) 19476–19484.